nature geoscience

PERSPECTIVE

PUBLISHED ONLINE: 1 MARCH 2017 | DOI: 10.1038/NGEO2876

Biotic and abiotic retention, recycling and remineralization of metals in the ocean

Philip W. Boyd[1,2]*, Michael J. Ellwood[3], Alessandro Tagliabue[4] and Benjamin S. Twining[5]

Trace metals shape both the biogeochemical functioning and biological structure of oceanic provinces. Trace metal biogeochemistry has primarily focused on modes of external supply of metals from aeolian, hydrothermal, sedimentary and other sources. However, metals also undergo internal transformations such as abiotic and biotic retention, recycling and remineralization. The role of these internal transformations in metal biogeochemical cycling is now coming into focus. First, the retention of metals by biota in the surface ocean for days, weeks or months depends on taxon-specific metal requirements of phytoplankton, and on their ultimate fate: that is, viral lysis, senescence, grazing and/or export to depth. Rapid recycling of metals in the surface ocean can extend seasonal productivity by maintaining higher levels of metal bioavailability compared to the influence of external metal input alone. As metal-containing organic particles are exported from the surface ocean, different metals exhibit distinct patterns of remineralization with depth. These patterns are mediated by a wide range of physicochemical and microbial processes such as the ability of particles to sorb metals, and are influenced by the mineral and organic characteristics of sinking particles. We conclude that internal metal transformations play an essential role in controlling metal bioavailability, phytoplankton distributions and the subsurface resupply of metals.

Trace metals such as iron set primary productivity across much of the ocean[1,2]. Other metals, including zinc and cobalt, play more targeted physiological roles linked to specific biogeochemical cycles[3,4]. Much emphasis in metal biogeochemistry has been placed on the identification of external supply mechanisms[5,6]. However in the case of iron, much of this supply — such as episodic dust plumes — may be chemically inaccessible[7] and/or biologically unavailable[8]. Long-standing investigations of nitrogen and phosphorus biogeochemistry[9] established that internal recycling through efficient biological retention sustains productivity. Likewise, solubilization of elements from sinking particles (termed remineralization) replenishes nutrient inventories at depth[10], which are seasonally resupplied to surface waters via mixing. Here, we exploit available insights to explore the abiotic and biotic mechanisms that underpin internal metal cycling: focussing on iron as the best-characterized metal[11], but drawing on illustrative examples for other metals. We contrast recycling patterns between trace- and macronutrients, and link the former to external supply mechanisms of metals to complete their biogeochemical cycles.

Trace metals have fundamentally different chemistry (speciation, reactivity, complexation[11]) than macronutrients[12], and thus have distinctive modes of external supply and internal recycling, with implications for the contribution of recycling versus external supply in supporting productivity (that is, the *f* ratio[12], see later). Additionally, macronutrients support macromolecular synthesis[12] whereas metals drive enzymatic catalysis[13]. These distinct metabolic roles probably account for different taxon-specific requirements for metals[14], a trend not evident for macronutrients[15]. Although some taxa target particular forms of macronutrients (for example, *Prochlorococcus*/ammonium; *Synechococcus*/nitrate[16]), such preferences are poorly defined for metals due to uncertainties such as how metal-binding ligands influence bioavailability[11].

We detail important advances across four specific themes: (1) pelagic iron retention and recycling; (2) the ratio of new to recycled iron and modes of supply; (3) observed versus modelled mesopelagic metal remineralization; and (4) controls on subsurface metal remineralization. Our understanding — catalysed by GEOTRACES[17] — has advanced substantially from prior reviews[18] (Supplementary Fig. 1) and we highlight insights from GEOTRACES process studies[19,20], surveys[8,21,22] and GEOTRACES-inspired modelling[23,24]; along with other recent[7,25,26] and prior (corroborative) research[27,28]. FeCycle II — a twelve-day quasi-Lagrangian GEOTRACES process study[19] characterized by an unprecedented combination of direct measurements of pelagic recycling[19,29] and subsurface metal remineralization[29,30] — serves to link our specific themes.

Drivers of pelagic metal retention and recycling

Retention of externally supplied metals by abiotic and biotic mechanisms within surface waters is a prerequisite for internal cycling (see Fig. 1). External supply largely occurs over the winter[31], with subsequent episodic supply[5,7]. For example, iron is initially retained in surface waters by excess ligands, a trend evident across GEOTRACES sections[22,32] regardless of the mode of external supply. Spring-time biological acquisition of iron[19,20] results in both the retention[29] and loss to depth[29,30] of this 'winter reserve' stock. Mechanisms including viral activity (lysis[19], ligands[33]) and grazing[19] internally mobilize this biologically retained iron. Abiotic mechanisms play a key role in retaining episodically supplied iron: from dust deposition[5] (or passing eddies[7]) through rapid 'cascades' between particulate and soluble forms[7], photochemically mediated dissolution of colloids[34] and the putative

[1]Institute for Marine and Antarctic Studies, University of Tasmania, Hobart TAS 7004, Australia. [2]Antarctic Climate and Ecosystems CRC, University of Tasmania, Battery Point TAS 7004, Australia. [3]Research School of Earth Sciences, The Australian National University, Canberra ACT 0200, Australia. [4]School of Environmental Sciences, University of Liverpool, Liverpool L69 3GP, UK. [5]Bigelow Laboratory for Ocean Sciences, East Boothbay, Maine 04544, USA. *e-mail: Philip.Boyd@utas.edu.au

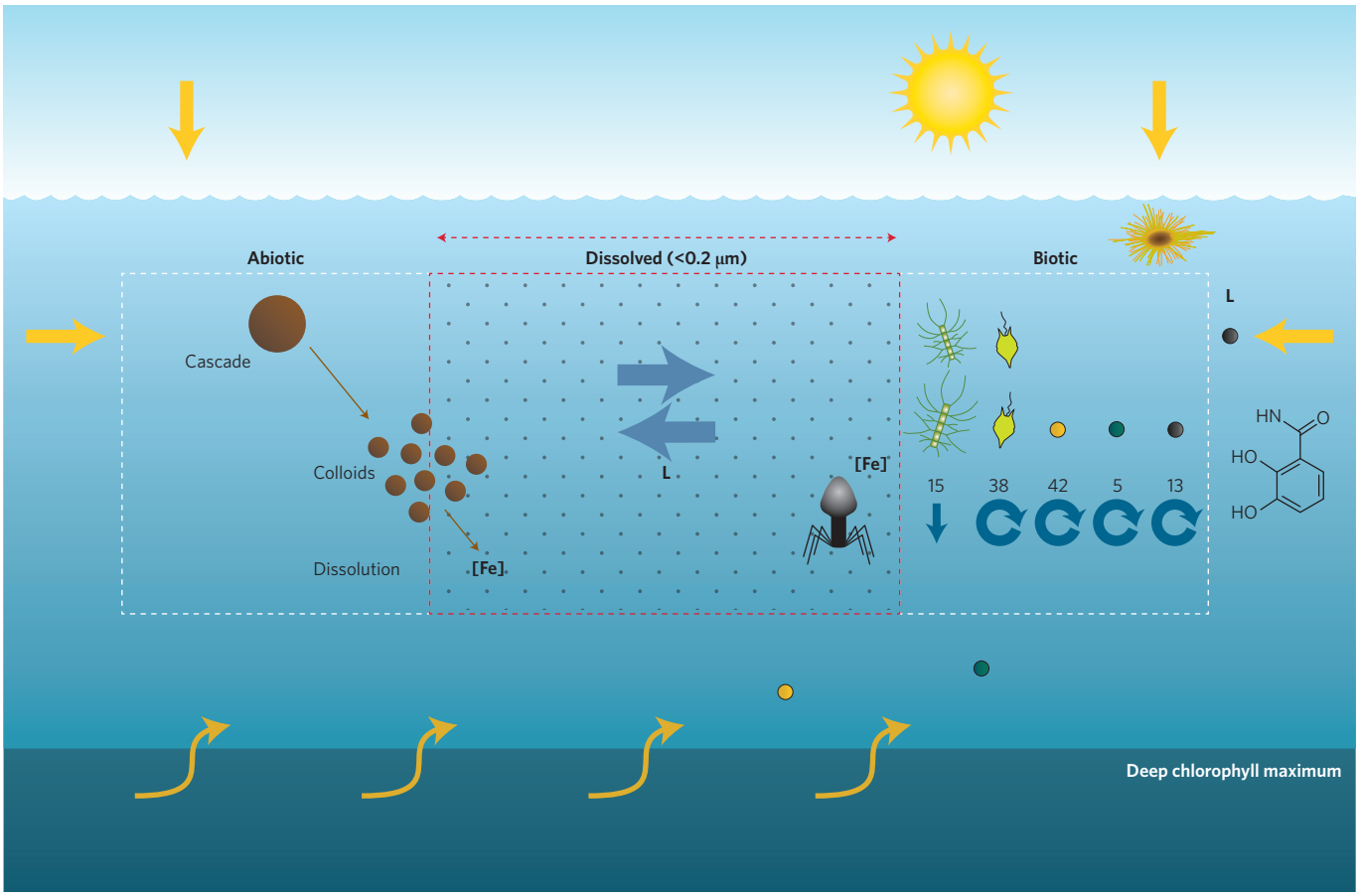

Figure 1 | Schematic of modes of 'new' iron supply (orange arrows) and iron retention mechanisms within the surface mixed layer. Abiotic retention (left box) includes rapid transfer of aerosol iron to soluble pools (that is, Cascade[7]) and photochemically mediated colloid dissolution[34]. Biotic retention (right box) is driven by acquisition (for example, aerosol capture by diazotrophs[36]) and interactions between iron supply, differing iron quotas (pmol l^{-1}) within natural communities (left-to-right: diatom[39], autotrophic flagellate[39], picoprokaryote[39], picoeukaryote[39], heterotrophic bacterium[39]) and their fate (export (downward blue arrow) or grazing/lysis (circular blue arrows)). Microbial ligand (L) release retains metals in solution (denoted by the partial chemical structure of the enterobactin siderophore) and is stimulated by new metal supply[25,26]. The virus represents putative iron recycling through progeny phages[33]. Horizontal blue arrows denote exchange between the dissolved and other pools mediated by ligands.

mechanism of transformation to inorganic iron colloids[21] (Fig. 1). Different supply modes influence taxon-specific biological acquisition strategies: episodic supply can stimulate microbial siderophore production[25,26], whereas aerosols are transformed by phagotrophy[35] and/or active transport (diazotrophs[36]), and vertical diffusive supply (potentially colloidal iron[7]) is targeted by phytoplankton at depth[37].

A major advance in understanding pelagic internal cycling (Supplementary Fig. 1) is determining how the biological ferrous wheel[38] is structured by the intersection of taxon-specific iron requirements[39] (such as quotas, total intracellular metal, mol per cell) and storage abilities[40], with distinct taxon-specific pathways and 'fates' of the biologically retained metal (such as grazing/lysis/sinking/cell death)[29] (Fig. 1). Hence, the wide-ranging acquisition strategies employed by phytoplankton[41] drive differences in the retention and recycling efficiency of each element. Other metals such as nickel have differing characteristics from iron that influence distinct physiological needs and acquisition (Supplementary Table 1). This range of acquisition mechanisms enables taxa with different metal requirements that arise from specific metabolic needs[13,39] (such as use-efficiencies[42] and/or cell sizes/abundances[29]) to coexist. A critical unknown is how abiotic and biotic retention mechanisms interact (Fig. 1). Although there have been major advances in elucidating abiotic[7,21,34] and biotic[25,26,29,33] retentive mechanisms, our understanding of the latter is more advanced. Ligands[25,26,33] may be a key linkage between mechanisms (Fig. 1), however additional pathways will probably connect abiotic and biotic processes, an emerging theme across geomicrobiology[43].

What proportion of 'new' trace metal inventories can be retained by biota? During FeCycle II[19], mixed-layer dissolved iron decreased from roughly 0.5 to 0.1 nmol l^{-1}, but the biotic iron inventory — based on quotas quantified with synchrotron X-ray fluorescence (SXRF) cell-mapping[8,30] — remained at approximately 0.1 nmol l^{-1} throughout and its rapid recycling extended seasonal productivity[19]. This study[19] suggests limits on the proportion of metal inventories that biota can access and recycle, which are probably constrained by temperature-dependent bounds on the growth/grazing rate and/or lags in predator–prey couplings (for example, the gut passage). Moreover, not all of the dissolved metal inventories may be available to all taxa[29].

New versus recycled metals and ocean productivity

The *fe* ratio describes the contribution of externally supplied iron to biological uptake relative to that supported by both externally supplied and internally cycled iron[44] and hence is analogous to the *f* ratio for nitrogen[12]. Calculation of the *fe* ratio requires detailed estimates of both biological iron demand and recycling

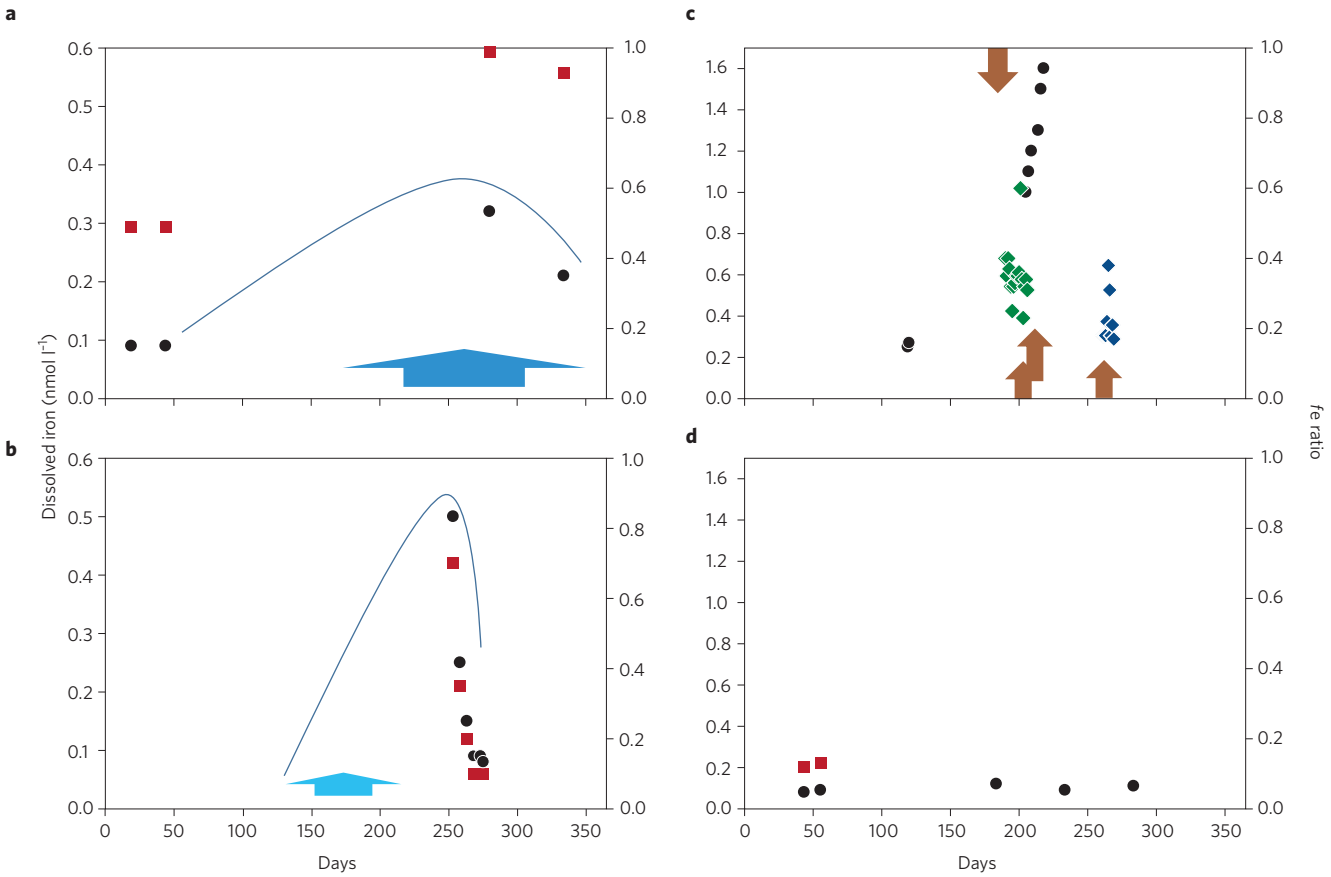

Figure 2 | Influence of different supply modes on surface mixed-layer iron (black) and the ratio of new versus recycled iron (red). a, Iron is mainly delivered to Kerguelen[20,45] from sustained deep-water supply (the blue arrow denotes estimated duration). **b**, Seasonally oligotrophic subtropical waters[19] from wintertime offshore lateral supply (blue arrow). **c**, Oligotrophic subtropical waters (Bermuda[28], black; Hawaii[7], green (2012 data set) and blue (2013) diamonds) from episodic dust supply (brown arrows). No *fe* ratio estimates were available. **d**, Low-iron subantarctic waters[44] during spring–summer aerosol deposition (days 250–100). In panels **a** and **b** observations were extrapolated (blue lines) based on projected seasonality in dissolved iron inventories[23].

(Supplementary Fig. 1). Emerging datasets from GEOTRACES process studies[19,20] enable the relationship between the *fe* ratio and different modes of supply to be probed (Fig. 2). Initial *fe* ratio estimates were from subantarctic low-iron waters where — despite invariant dissolved iron vertical profiles — approximately 90% of productivity was fuelled by internal cycling[44].

A major advance is the recognition that *fe* ratios change with locale, season and regional inventories (Supplementary Fig. 1). Recycled iron is less important in high-iron waters sustained by upwelling[20,45] compared with that supplied by transient winter-reserves (Fig. 2a,b). *fe* ratios of ~1 were evident off the Kerguelen Islands at the onset of the diatom bloom[20], and were approximately 0.5 after more than one month of bloom development[45]. In contrast, subtropical Pacific waters[29] revealed rapid removal of externally supplied iron (that is, decreased *fe* ratios) during the transition to summer oligotrophy (Fig. 2b).

Summer iron stocks are enhanced in subtropical Atlantic and Pacific waters via episodic dust inputs (Fig. 2c). Sustained high iron[7,28] suggests either a biological surfeit (that is, indicative of high *fe* ratios, no available data) or that this iron is chemically inactive[7,8] or biologically inaccessible[8] due to light and/or phosphate limitation[2]. Despite regional differences in dissolved iron stocks and *fe* ratios (Fig. 2), surprising uniformity in biotic iron inventories emerges across contrasting sites[29]. This raises some questions: can recycled iron (supplying 50–90% of demand) subsidize cells with high requirements (for example, picoprokaryotes[39])? And if some taxa target episodically supplied iron (Fig. 1), do others focus on recycled forms? If so, does iron speciation dictate such taxon specialization?

Subsurface remineralization length scales

Sinking particles fuel the biological pump, and transformations attenuate particle flux with depth, replenishing dissolved nutrients[10] and setting nutricline depths[31]. Remineralization length scales — that is, the attenuation (at some rate k (s^{-1})) of the downward particulate flux of an element settling gravitationally (speed ω (m s^{-1}) is defined by ω K^{-1} (m)) — vary among major elements, causing vertical decoupling at depth[10]. Length scales also vary between metals (Table 1). Remineralization length scales are generally longer for metals, relative to macronutrients[27], as metals comprise both lithogenic (relatively refractory) and biogenic (labile) components of sinking heterogeneous particles (Fig. 3). Indeed, for copper, the sinking flux is essentially a 'lithogenic throughput' with little flux attenuation (Supplementary Table 1). Hence, directly comparing remineralization length scales between elements in heterogeneous particles is problematic.

A study targeting export from a diatom-dominated bloom[30] circumvented the lithogenic influence on remineralization by focusing analytically on diatoms. Two-dimensional elemental maps of the dominant diatom species revealed depth-dependent elemental shifts in the cellular and structural components (Supplementary Fig. 2a; Fig. 3a). Significant differences between

Table 1 | Synthesis of remineralization length scales of trace metals and major elements in the ocean.

Element	*b* value	Relative difference (scaled to POC)	Regeneration processes and factors	Particle assemblage	Region
N	1.68 ± 0.13	1.34	R, [O], Re	All	NPSG[27]
POC	1.25 ± 0.09	1	R, [O], M	All	NPSG
C*	1.09 ± 0.60	1	R, [O], M	Diatoms	New Zealand (S. Pacific)[30]
P	0.88 ± 0.48	0.70	R	All	NPSG
P	0.63 ± 0.28	0.58	R	Diatoms	S. Pacific
BSi	0.22 ± 0.53	0.18	R, OC	All	NPSG
Si	0.12 ± 0.11	0.11	R, OC	Diatoms	S. Pacific
Zn	0.77 ± 0.34	0.70	R, Cx?	Diatoms	S. Pacific
Ni	0.90 ± 0.76	0.83	R	Diatoms	S. Pacific
Al	0.52 ± 0.29	0.42	R, S	All	NPSG
Fe	0.32 ± 0.28	0.07	R, S, Re, Cx	All	NPSG
Fe	0.13 ± 0.17	0.12	R, S, Re, Cx	Diatoms	S. Pacific
Cu	0.09 ± 0.38	0.07	R, S?, Re?	All	NPSG

Length scales are expressed as (positive) *b* values (that is, higher values denote shorter length scales) using power-law fitting of the vertical attenuation in particle flux[50]. Values are from observed sinking flux of all particles: that is, lithogenic/biogenic (150–500 m depth)[27]; and diatoms (50–200 m)[30]. *S as a C proxy. POC, particulate organic carbon; Cx, complexation; BSi, biogenic silica; R, remineralization; [O], oxygen concentration; Re, redox state; M, molecular lability; S, scavenging/sorption; OC, organic coatings; NPSG, North Pacific subtropical gyre. The question marks denote uncertainties.

remineralization of major elements (for example, sulfur and silicon) and between trace elements (for example, iron and zinc) emerged (Table 1). Such studies[27,30] use the power of spatial associations between elements in individual particles to explore if remineralization patterns are coupled (Supplementary Fig. 2a,b). Spatial co-location between major elements was evident in surface waters only, indicative of selective remineralization and decoupling in the breakdown of major and trace elements with depth[30]. These advances provide the detailed mechanisms needed to better understand basin-scale cycling of major and trace elements using global ocean models (Supplementary Fig. 1).

Observed remineralization length scales are compared with state-of-the-art model simulations[23] in Table 2. PISCES[23] reflects observed trends in remineralization (carbon/phosphorus length scales < iron < silicon), but simulates a shorter length scale globally for iron than is observed (Table 2). As iron remineralization in all current models[23,24] is tied to phosphorus, the roughly twofold longer remineralization length scale for iron versus phosphorus arises *in silico* from additional scavenging and colloidal pumping of remineralized iron onto particles. Observations suggest that models underestimate iron remineralization length scales by four- to tenfold (Tables 1 and 2), affecting projections of nutrient resupply stoichiometry and ferricline depth[31] (Supplementary Table 1). Future models must consider additional factors including distinct particulate pools (for example, biogenic/lithogenic) in setting remineralization length scales.

Subsurface controls on metal remineralization

A better understanding of why element nutriclines vary[31] requires mechanisms to decouple remineralization (Supplementary Table 1). For macronutrients, mechanisms include preferential microbially mediated nitrogen remineralization (compared to carbon) to meet nutritional requirements[46]. Element associations with different cellular components (for example, membranes) probably influence their targeted regeneration by substrate-specific bacterial enzymes (Fig. 3a). For sinking diatoms[30], more cellular P/Ni/Zn/S was remineralized compared to iron (suggesting re-adsorption due to iron's high particle reactivity[47]) and silicon (no bacterial demand means dissolution requires prior carbon solubilization[48]) by 200 m. This study[30] provides novel linkages between elements, their biochemical role, cellular location, metal-specific microbial enzymes, and hence differential, targeted remineralization (Supplementary Figs 1,2).

Heterogeneous particles often dominate the sinking assemblage but are difficult to study individually (Supplementary Fig. 2b,c). Figure 3 offers a conceptual approach to jointly consider disparate biotic/abiotic mechanisms (with parallels in geomicrobiology[43]) used independently to derive chemical[49] or biological[50] rate constants for particle breakdown. The fates of particulate biogenic iron, zinc and phosphorus diverge (Fig. 3) because they each may encounter a range of different biological (solubilization) and physical ((dis)aggregation) transformation mechanisms — iron, for example, probably sorbs onto (that is, scavenged) and desorbs from particles[47,49]. Moreover, once desorbed, iron can be re-sorbed onto particles[49] and/or consumed (for example, by particle-attached bacteria). It is also highly probably that abiotically scavenged iron can be remobilized by particle-associated grazers (see Supplementary Movie; Fig. 3), illustrating how abiotic/biotic transformations interact[43]. This combination of abiotic and biotic processes, along with the refractory nature of lithogenic iron[8] (Supplementary Fig. 2b) help explain why iron often has longer remineralization length scales than other elements. As many processes jointly set remineralization length scales of different elements, incorporating this level of detail into biogeochemical models to more accurately simulate the stoichiometry of nutrient supply is a major future challenge.

Teasing apart abiotic and biotic transformations

Advances in understanding internal cycling and remineralization indicate that bioactive metals are characterized by more complex transformations than for major elements. Hence, elucidating the individual and interactive effects of biological and chemical transformations on cycling and remineralization represents a major challenge. In surface waters, a key goal is to differentiate the roles of phytoplankton and microbes (such as their differing metal quotas and fates), and the function of ligands in setting the taxon-specific bioavailability and/or kinetic constraints on the specific acquisition pathways for recycled versus 'new' metals.

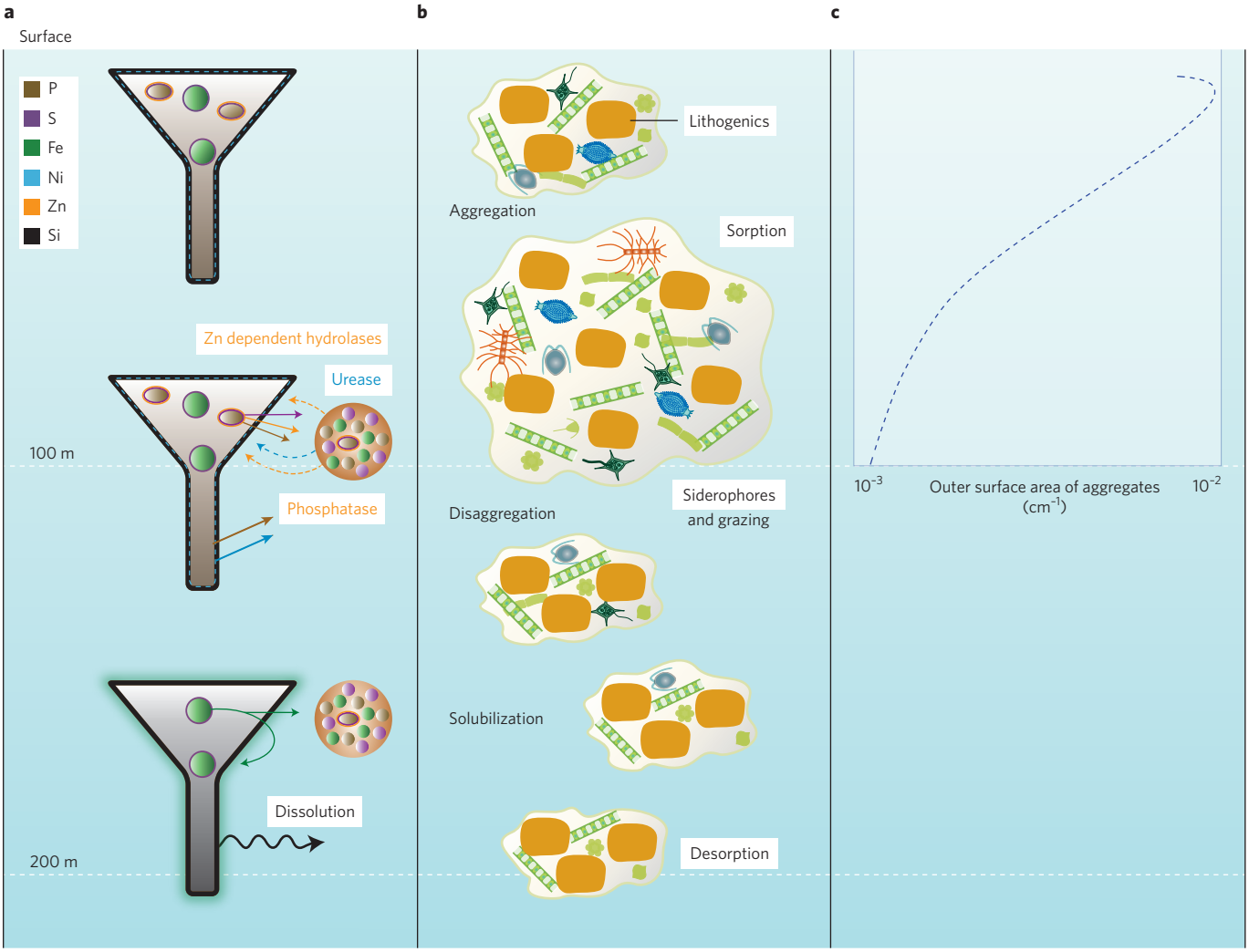

Figure 3 | Mechanisms that set the different remineralization length scales evident for trace metals and major elements. a, Hypothetical remineralization mechanisms for a sinking diatom (six-sided polygon) based on SXRF element mapping[30] (S is a C proxy[30,39]). Preferential subsurface regeneration of elements is linked to their association with structural/biochemical cellular components (for example, membranes) and microbial elemental requirements (circles). **b**,**c**, Idealized processes acting on sinking heterogeneous particles (lithogenic/biogenic components with different labilities). Particle transformations drive remineralization (**b**, highlighted terms are metal specific) and depth-dependent changes in particle aggregate surface area (**c**, bio-optical profiling float data, courtesy of George Jackson), which influences local chemistry and microbial processes (see Supplementary Movie).

Table 2 | Synthesis of modelled remineralization length scales of trace metals and major elements in the ocean.

Element	*b* value	Relative difference (scaled to POC)	Regeneration processes and factors	Particle assemblage	Region
POC	1.65 ± 0.57	1	R, [O]	All	Global ocean > 1000 m depth
POP*	1.65 ± 0.57	1	R, [O]	All	Global ocean > 1000 m depth
BSi	0.24 ± 0.05	0.15	R	All	Global ocean > 1000 m depth
PFe	0.88 ± 0.32	0.53	R, [O], S	All	Global ocean > 1000 m depth

Length scales are expressed as (positive) *b* values (that is, higher values denote shorter length scales) using power-law fitting of the vertical attenuation in particle flux[50]. Remineralization length scales from biogeochemical simulations (100–1000 m) using PISCES[23]. *POC and POP are interchangeable in model runs. POC, particulate organic carbon; POP, particulate organic phosphorus; BSi, biogenic silica; PFe, particulate iron; R, remineralization; [O], oxygen concentration; S, scavenging/sorption.

These processes set the degree of metal retention and recycling (versus export). Research into iron is most advanced, but we contend that this cannot be used as a biogeochemical template for all trace metals. Other metals, often with different characteristics linked with unique biochemical roles[8,13] and taxon-specific needs[39], require dedicated study and modelling.

At depth, mixed lithogenic/biogenic particle populations and their varying degrees of metal remobilization, pose a major challenge to determine whether sinking particles mainly represent a throughput of metals to depth or a vector for the replenishment of dissolved metal inventories (in conjunction with the essential resupply of ligands that retain the metals in solution[17]). The

specific fate of elements within particles also influences the coupling between major and trace elements. Elemental and isotopic mapping of particles — along with biogeochemical models — are powerful approaches to tease apart this puzzle. However, models currently focus on large scales[24], limiting their utility in exploring underlying biogeochemical processes in detail. We advocate a parallel approach, whereby the next generation of biogeochemical models are used within simplified physical oceanographic frameworks to develop new representations of metal cycling and assess the biogeochemical significance of these complex transformations. Models would then reflect both the progress in understanding external sources of metals[5,6], their biogeochemical cycling and the associated return pathways — encapsulated by the term remineralization — in the oceans' interior.

Methods

Methods, including statements of data availability and any associated accession codes and references, are available in the online version of the paper.

Received 13 June 2016; accepted 8 December 2016; published online 1 March 2017

References

1. Boyd, P. W. *et al.* Mesoscale iron enrichment experiments 1993–2005: synthesis and future directions. *Science* **315,** 612–617 (2007).
2. Moore, C.M. *et al.* Processes and patterns of oceanic nutrient limitation. *Nat. Geosci.* **6,** 701–710 (2013).
3. Cullen, J. T. & Sherrell, R. M. Effects of dissolved carbon dioxide, zinc, and manganese on the cadmium to phosphorus ratio in natural phytoplankton assemblages. *Limnol. Oceanogr.* **50,** 1193–1204 (2005).
4. Koch, F. *et al.* The effect of vitamin B12 on phytoplankton growth and community structure in the Gulf of Alaska. *Limnol. Oceanogr.* **56,** 1023–1034 (2011).
5. Jickells, T. D. & C. M. Moore. The importance of atmospheric deposition for oceanic productivity. *Annu. Rev. Ecol. Evol. Syst.* **46,** 481–501 (2015).
6. Resing, J. A. *et al.* Basin-scale transport of hydrothermal dissolved metals across the South Pacific Ocean. *Nature* **523,** 200–203 (2015).
7. Fitzsimmons, J. N. *et al.* Daily to decadal variability of size-fractionated iron and iron-binding ligands at the Hawaii Ocean Time-series Station ALOHA. *Geochim. Cosmochim. Acta* **171,** 303–324 (2015).
8. Twining, B. S., Rauschenberg, S., Morton, P. & Vogt, S. Metal contents of phytoplankton and labile particulate material in the North Atlantic Ocean. *Prog. Oceanogr.* **137,** 261–293 (2015).
9. Karl, D. M. *et al.* in *Ocean Biogeochemistry: The Role of the Ocean Carbon Cycle in Global Change* (ed. Fasham, M. J. R.) Ch. 11 (Springer, 2003).
10. Weber, T., Cram, J. A., Leung S. W., DeVries T. & Deutsch C. Deep ocean nutrients imply large latitudinal variation in particle transfer efficiency. *Proc. Natl Acad. Sci. USA* **113,** 8606–8611 (2016).
11. Bruland, K. W. & Lohan, M. C. in *The Oceans and Marine Geochemistry: Treatise on Geochemistry* (ed. Elderfield, H.) Ch. 6 (Elsevier, 2003).
12. Zehr, J. P. & Ward, B. B. Nitrogen cycling in the ocean: new perspectives on processes and paradigms. *Appl. Environ. Microbiol.* **68,** 1015–1024 (2002).
13. Morel, F. M. M. & Price, N. M. The biogeochemical cycles of trace metals in the oceans. *Science* **300,** 944–947 (2003).
14. Quigg, A., Irwin, A. J. & Finkel, Z. V. Evolutionary inheritance of elemental stoichiometry in phytoplankton. *Proc. R. Soc. Lond. B* **278,** 526–534 (2011).
15. Singh, A., Baer, S. E., Riebesell, U., Martiny, A. C. & Lomas, M. W. C : N : P stoichiometry at the Bermuda Atlantic Time-series Study station in the North Atlantic Ocean. *Biogeosciences* **12,** 6389–6403 (2015).
16. Martiny, A. C., Kathuria, S. K. & Berube P. Widespread metabolic potential for nitrite and nitrate assimilation among *Prochlorococcus* ecotypes. *Proc. Natl Acad. Sci. USA* **106,** 10787–10792 (2009).
17. http://www.geotraces.org/
18. Boyd, P. W. & Ellwood, M. J. The biogeochemical cycle of iron in the ocean. *Nat. Geosci.* **3,** 675–682 (2010).
19. Boyd, P. W. *et al.* Microbial control of diatom bloom dynamics in the open ocean. *Geophys. Res. Lett.* **39,** L18601 (2012).
20. Bowie. A. R. *et al.* Iron budgets for three distinct biogeochemical sites around the Kerguelen Archipelago (Southern Ocean) during the natural fertilisation study, KEOPS-2. *Biogeosciences* **12,** 4421–4445 (2015).
21. Fitzsimmons, J. N., Bundy, R. M., Al-Subiai, S. N., Barbeau, K. A. & Boyle, E. A. The composition of dissolved iron in the dusty surface ocean: an exploration using size-fractionated iron-binding ligands. *Mar. Chem.* **173,** 125–135 (2015).
22. Buck, K. N., Sohst B. & Sedwick, P. N. The organic complexation of dissolved iron along the US GEOTRACES (GA03) North Atlantic Section. *Deep-Sea Res. PT II.* **116,** 152–165 (2015).
23. Aumont, O., Ethé, C., Tagliabue, A., Bopp, L. & Gehlen, M. PISCES-v2: an ocean biogeochemical model for carbon and ecosystem studies. *Geosci. Model Dev.* **8,** 2465–2513 (2015).
24. Tagliabue, A. *et al.* How well do global ocean biogeochemistry models simulate dissolved iron distributions? *Global Biogeochem. Cy.* **30,** GB005289 (2016).
25. Adly, C. L. *et al.* Response of heterotrophic bacteria to mesoscale iron enrichment in the northeast subarctic Pacific Ocean. *Limnol. Oceanogr.* **60,** 136–148 (2015).
26. Bundy R. M., Jiang, M., Carter, M & Barbeau, K. A. Iron-binding ligands in the southern California current system: mechanistic studies. *Front. Mar. Sci.* **3,** 27 (2016).
27. Lamborg, C. H., Buesseler, K. O. & Lam, P. J. Sinking fluxes of minor and trace elements in the North Pacific Ocean measured during the VERTIGO program. *Deep-Sea Res. PT II* **55,** 1564–1577 (2008).
28. Sedwick, P. N. *et al.* Iron in the Sargasso Sea (Bermuda Atlantic Time-series Study region) during summer: eolian imprint, spatiotemporal variability, and ecological implications. *Global Biogeochem. Cy.* **19,** GB4006 (2005).
29. Boyd, P. W. *et al.* Why are biotic iron pools uniform across high- and low-iron pelagic ecosystems? *Global Biogeochem. Cy.* **29,** 1028–1043 (2015).
30. Twining, B. S. *et al.* Differential remineralization of major and trace elements in sinking diatoms. *Limnol. Oceanogr*. **59,** 689–704 (2014).
31. Tagliabue, A., Sallee, J.-B., Bowie, A. R., Levy, M., Swart, S. & Boyd, P. W. Surface-water iron supplies in the Southern Ocean sustained by deep winter mixing. *Nat. Geosci.* **7,** 314–320 (2014).
32. Boyd, P. W. & Tagliabue, A. Using the L* concept to explore controls on the relationship between paired ligand and dissolved iron concentrations in the ocean. *Mar. Chem.* **173,** 52–66 (2015).
33. Bonnain, C., Breitbart, M & Buck, K. N. The ferrojan horse hypothesis: iron-virus interactions in the ocean. *Front. Mar. Sci.* **3,** 82 (2016).
34. Wells, M. L., Mayer, L. M., Donard, O. F. X., de Souza Sierra, M. M. & Ackelson, S. G. The photolysis of colloidal iron in the oceans. *Nature* **353,** 248–250 (1991).
35. Barbeau, K. A. & Moffett, J. W. Dissolution of iron oxides by phagotrophic protists: using a novel method to quantify reaction rates. *Environ. Sci. Technol.* **32,** 2969–2975 (1998).
36. Rubin, M., Berman-Frank, I. & Shaked, Y. Dust-and mineral-iron utilization by the marine dinitrogen-fixer *Trichodesmium*. *Nat. Geosci.* **4,** 529–534 (2011).
37. Hopkinson, B. M. & Barbeau, K. Interactive influences of iron and light limitation on phytoplankton at subsurface chlorophyll maxima in the eastern North Pacific. *Limnol. Oceanogr.* **53,** 1303–1318 (2008).
38. Kirchman D. L. Microbial ferrous wheel. *Nature* **383,** 303–304 (1996).
39. Twining, B. S. & Baines S. B. The trace metal composition of marine phytoplankton. *Annu. Rev. Mar. Sci.* **5,** 191–215 (2013).
40. Marchetti, A. *et al.* Ferritin is used for iron storage in bloom-forming marine pennate diatoms. *Nature* **457,** 467–470 (2009).
41. Lis, H., Shaked, Y., Kranzler, C. Keren N. & Morel, F. M. M. Iron bioavailability to phytoplankton: an empirical approach. *The ISME Journal* **9,** 1003–1013 (2015).
42. Sunda W. G. & Huntsman S. A. Iron uptake and growth limitation in oceanic and coastal phytoplankton. *Mar. Chem.* **50,** 189–206 (1995).
43. Melton, C. D., Swanner, E. D., Behrens, S., Schmidt C. & Kappler, A. The interplay of microbially mediated and abiotic reactions in the biogeochemical Fe cycle. *Nat. Rev. Micro.* **12,** 797–808 (2014).
44. Boyd P. W. *et al.* FeCycle: attempting an iron biogeochemical budget from a mesoscale SF6 tracer experiment in unperturbed low iron waters. *Global Biogeochem. Cy.* **19,** GB002494 (2005).
45. Sarthou, G. *et al.*, The fate of biotic iron during a phytoplankton bloom induced by natural fertilization: Impact of copepod grazing. *Deep-Sea Res. PT II* **55,** 734–751 (2008).
46. Smith, D. C., Simon, M., Alldredge, A. L. & Azam F. Intense hydrolytic enzyme activity on marine aggregates and implications for rapid particle dissolution. *Nature* **359,** 139–142, (1992).
47. Frew, R. D. *et al.* Particulate iron dynamics during FeCycle in subantarctic waters southeast of New Zealand. *Global Biogeochem. Cy.* **20,** GB002558 (2006).
48. Bidle, K. D. & Azam, F. Accelerated dissolution of diatom silica by marine bacterial assemblages. *Nature* **397,** 508–512 (1999).

49. Clegg, S. L. & Whitfield, M. A generalized model for the scavenging of trace metals in the open ocean—II. Thorium scavenging. *Deep-Sea Res.* **38,** 91–120 (1991).
50. Boyd, P. W. & Trull, T. W. Understanding the export of biogenic particles in oceanic waters: is there consensus? *Prog. Oceanogr.* **72,** 276–312 (2007).

Acknowledgements

The authors thank G. Jackson (Texas A&M University) and T. Kiørboe (Technical University of Denmark) for the provision of unpublished data/video footage. The authors acknowledge the role of collaborations with David Hutchins, Sylvia Sander, Robert Strzepek and Steve Wilhelm in developing this Perspective. The sinking particles presented in Supplementary Fig. 2c were collected by Z. Baumann (University of Connecticut) and analysed with the assistance of D. Ohnemus (Bigelow Laboratory for Ocean Sciences). This analysis used resources of the Advanced Photon Source, a US Department of Energy (DOE) Office of Science User Facility operated for the DOE Office of Science by Argonne National Laboratory under Contract No. DE-AC02-06CH11357. Support was provided by Australian Research Council Australian Laureate Fellowship project FL160100131 and Antarctic Climate and Ecosystems Cooperative Research Centre funding to P.W.B., an Australian Research Council Discovery Project DP130100679 to M.J.E. and P.W.B. B.S.T. was supported by US National Science Foundation grant OCE-1232814. Model simulations by A.T. are supported by N8 HPC Centre of Excellence, provided and funded by the N8 consortium and EPSRC (Grant No. EP/K000225/1).

Author contributions

P.W.B., M.J.E., A.T. and B.S.T. contributed equally to conceiving and developing the material presented, and to writing the paper.

Additional information

Supplementary information is available in the online version of the paper. Reprints and permissions information is available online at www.nature.com/reprints. Correspondence and requests for materials should be addressed to P.B.

Competing financial interests

The authors declare no competing financial interests.

Methods

Collection of aggregate image (displayed in Supplementary Fig. 2c). The aggregate was collected from 15 m depth in eastern Long Island Sound using an acid-washed GO-FLO bottle. Particulate aggregates in whole water were settled by gravity into small centrifuge tubes and frozen at −20 °C. Samples were subsequently thawed, and particles gently collected onto acid-washed 10 μm pore-sized polycarbonate Isopore membrane filters (Millipore). Unrinsed filters were frozen at −20 °C prior to freeze drying for 24 h. Aggregates were analysed with synchrotron X-ray fluorescence (SXRF) microscopy at GEOCARS beamline 13IDE at Advanced Photon Source. Samples were held in a He environment and scanned with 10.5 keV incident X-rays focused to approximately 2 μm spot with Kirkpatrick-Baez mirrors. A dwell time of 200 msec at each pixel was used.